Exploring the Thermodynamics of a Universal Fermi Gas

Sylvain Nascimbène, Nir Navon, Kaijun Jiang, Frédéric Chevy, Christophe Salomon

Exploring the thermodynamics of a universal Fermi gas

S. Nascimbène, N. Navon, K. J. Jiang, F. Chevy, and C. Salomon
Laboratoire Kastler Brossel, CNRS,
UPMC, École Normale Supérieure,
24 rue Lhomond, 75231 Paris, France

PACS numbers: 03.75.Ss; 05.30.Fk; 32.30.Bv; 67.60.Fp

From sand piles to electrons in metals, one of the greatest challenges in modern physics is to understand the behavior of an ensemble of strongly interacting particles. A class of quantum many-body systems such as neutron matter and cold Fermi gases share the same universal thermodynamic properties when interactions reach the maximum effective value allowed by quantum mechanics, the so-called unitary limit [1, 2]. It is then possible to simulate some astrophysical phenomena inside the highly controlled environment of an atomic physics laboratory. Previous work on the thermodynamics of a two-component Fermi gas led to thermodynamic quantities averaged over the trap [3–5], making it difficult to compare with many-body theories developed for uniform gases. Here we develop a general method that provides for the first time the equation of state of a uniform gas, as well as a detailed comparison with existing theories [6–15]. The precision of our equation of state leads to new physical insights on the unitary gas. For the unpolarized gas, we show that the low-temperature thermodynamics of the strongly interacting normal phase is well described by Fermi liquid theory and we localize the superfluid transition. For a spin-polarized system [16–18], our equation of state at zero temperature has a 2% accuracy and it extends the work of [19, 20] on the phase diagram to a new regime of precision. We show in particular that, despite strong interactions, the normal phase behaves as a mixture of two ideal gases: a Fermi gas of bare majority atoms and a non-interacting gas of dressed quasi-particles, the fermionic polarons [10, 18, 20–22].

In this letter we study the thermodynamics of a mixture of the two lowest spin states ($i = 1, 2$) of ^{6}Li prepared at a magnetic field $B = 834$ G (see Methods), where the dimensionless number $1/k_F a$ characterizing the s-wave interaction is equal to zero, the unitary limit. k_F is the Fermi momentum and a the scattering length. Understanding the universal thermodynamics at unitarity is a challenge for many-body theories because of the strong interactions between particles. Despite this complexity at the microscopic scale, all the macroscopic properties of an homogeneous system are encapsulated within a single equation of state $P(\mu_1, \mu_2, T)$ that relates the pressure P of the gas to the chemical potentials μ_i of the species i and to the temperature T. In the unitary limit, this relationship can be expressed as [1]:

$$P(\mu_1, \mu_2, T) = P_1(\mu_1, T) h\left(\eta = \frac{\mu_2}{\mu_1}, \zeta = \exp\left(\frac{-\mu_1}{k_B T}\right)\right), \quad (1)$$

where $P_1(\mu_1, T) = -k_B T \lambda_{dB}^{-3}(T) f_{5/2}\left(-\zeta^{-1}\right)$ is the pressure of a single component non-interacting Fermi gas and $f_{5/2}(z) = \sum_{n=1}^{\infty} z^n/n^{5/2}$. $h(\eta, \zeta)$ is a universal function which contains all the thermodynamic information of the unitary gas (Fig. 1). In cold atomic systems, the inhomogeneity due to the trapping potential makes the measurement of $h(\eta, \zeta)$ challenging. However, this inhomogeneity of the trap can be turned into an advantage as shown in [20, 23].

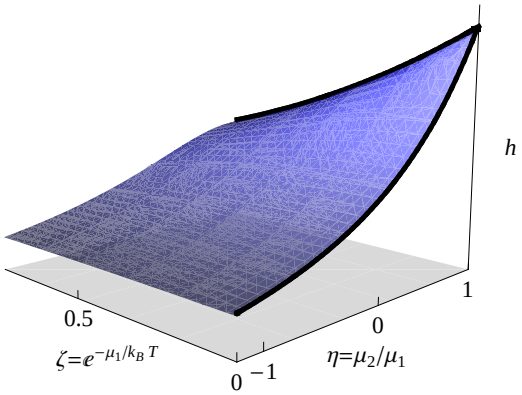

FIG. 1: Schematic representation of the universal function $h(\eta, \zeta)$. It fully describes the thermodynamics of the unitary gas as a function of chemical potential imbalance $\eta = \mu_2/\mu_1$ and of the inverse of the fugacity $\zeta = \exp(-\mu_1/k_B T)$. In this paper we measure the function h over the black lines $(1, \zeta)$ and $(\eta, 0)$ which correspond to the balanced unitary gas at finite temperature and to the spin-imbalanced gas at zero temperature, respectively.

We directly probe the local pressure of the trapped gas using *in situ* images, following the recent proposal [23]. In the local density approximation, the gas is locally homogeneous with local chemical potentials:

$$\mu_i(\mathbf{r}) = \mu_i^0 - V(\mathbf{r}) \quad (2)$$

(μ_i^0 is the chemical potential at the bottom of the trap for species i). Then a simple formula relates the pressure P to the doubly-integrated density profiles [23]:

$$P(\mu_{1z}, \mu_{2z}, T) = \frac{m\omega_r^2}{2\pi}\left(\overline{n}_1(z) + \overline{n}_2(z)\right), \quad (3)$$

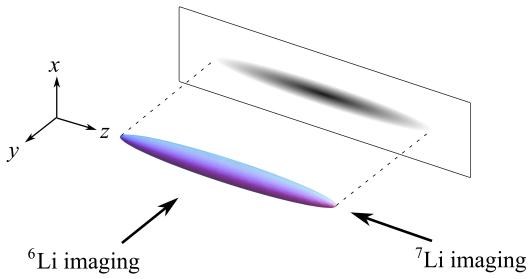

FIG. 2: Schematic representation of our atomic sample. The ^{6}Li atomic cloud is imaged in the direction y; the column density is then integrated along the direction x to give $\overline{n}(z)$. The ^{7}Li atoms are imaged after a time of flight along the z direction.

where $\overline{n}_i(z) = \int n_i(x,y,z)\mathrm{d}x\mathrm{d}y$, n_i being the atomic density. ω_r (resp. ω_z) is the transverse (resp. axial) angular frequency of a cylindrically symmetric trap (see Fig. 2) and $\mu_{iz} = \mu_i(0,0,z)$ is the local chemical potential along the z axis. From a single image, we thus measure the equation of state (1) along the parametric line $(\eta,\zeta) = (\mu_{2z}/\mu_{1z}, \exp(-\mu_{1z}/k_BT))$, see below.

The interest of this method is straightforward. First, one directly measures the equation of state (EOS) of the uniform gas. Second, each pixel row z_i gives a point $h(\eta(z_i),\zeta(z_i))$ whose signal to noise ratio is essentially given by the one of $\overline{n}_1(z) + \overline{n}_2(z)$; typically one experimental run leads to ~ 100 points with a signal to noise between 3 and 10. With about 40 images one gets $\simeq 4000$ points $h(\eta,\zeta)$, which after averaging provides a low-noise EOS of standard deviation $\sigma = 2\%$. In the following we illustrate the efficiency of our method on two important sectors of the parameter space (η,ζ) in Fig. 1: the balanced gas at finite temperature $(1,\zeta)$ and the zero-temperature imbalanced gas $(\eta,0)$.

We first measure the equation of state of the unpolarized unitary gas at finite temperature, $P(\mu_1,\mu_2,T) = P(\mu,T)$. The measurement of $h(1,\zeta)$ through the local pressure (3) can be done provided one knows the temperature T of the cloud and its central chemical potential μ^0.

In the balanced case, model-independent thermometry is notoriously difficult because of the strong interactions. Inspired by [24], we overcome this issue by measuring the temperature of a ^{7}Li cloud in thermal equilibrium with the ^{6}Li mixture (see Methods).

μ^0 is fitted on the hottest clouds so that the EOS agrees in the classical regime $\zeta \gg 1$ with the second-order virial expansion $h(1,\zeta) \simeq 2(1+\zeta^{-1}/\sqrt{2})$ [25]. For colder clouds we proceed recursively. The EOS of an image recorded at temperature T has some overlap with the previously determined EOS from all images with $T' > T$. In this overlap region μ^0 is fitted to minimize the distance between the two EOS's. This provides a new portion of the EOS at lower temperature. Using 40 images of clouds prepared at different temperatures, we thus reconstruct a low-noise EOS from the classical part down to the degenerate regime, as shown in Fig. 3a.

We now comment the main features of the equation of state. At high temperature, the EOS can be expanded in powers of ζ^{-1} as a virial expansion [11]:

$$\frac{h(1,\zeta)}{2} = \frac{\sum_{k=1}^{\infty}\left((-1)^{k+1}k^{-5/2} + b_k\right)\zeta^{-k}}{\sum_{k=1}^{\infty}(-1)^{k+1}k^{-5/2}\zeta^{-k}},$$

where b_k is the k^{th} virial coefficient. Since we have $b_2 = 1/\sqrt{2}$ in the measurement scheme described above, our data provides for the first time the experimental values of b_3 and b_4. $b_3 = -0.35(2)$ is in excellent agreement with the recent calculation $b_3 = -0.291 - 3^{-5/2} = -0.355$ from [11] but not with $b_3 = 1.05$ from [12]. $b_4 = 0.096(15)$ involves the 4-fermion problem at unitarity and could interestingly be computed along the lines of [11].

Let us now focus on the low-temperature regime of the normal phase $\zeta \ll 1$. As shown in Fig. 3b, we observe a T^2 dependence of the pressure with temperature. This behavior is reminiscent of a Fermi liquid and indicates that pseudogap effects expected for strongly-interacting Fermi superfluids [26] do not show up at the thermodynamic level within our experimental precision. In analogy with ^{3}He or heavy-fermion metals, we fit our data with the EOS:

$$P(\mu,T) = 2P_1(\mu,0)\left(\xi_n^{-3/2} + \frac{5\pi^2}{8}\xi_n^{-1/2}\frac{m^*}{m}\left(\frac{k_BT}{\mu}\right)^2\right), \quad (4)$$

$P_1(\mu,0) = 1/15\pi^2(2m/\hbar^2)^{3/2}\mu^{5/2}$ being the pressure of a single-component Fermi gas at zero temperature. m^* is the quasi-particle mass and ξ_n^{-1} is the compressibility of the normal gas extrapolated to zero temperature, and normalized to that of an ideal gas of same density. We deduce two new parameters $m^*/m = 1.13(3)$ and $\xi_n = 0.51(2)$. Despite the strong interactions m^* is close to m, unlike the weakly interacting ^{3}He liquid for which $2.7 < m^*/m < 5.8$, depending on pressure. Our ξ_n value is in agreement with the variational Fixed-Node Monte-Carlo calculations $\xi_n = 0.54$ in [27], $\xi_n = 0.56$ in [10] and with the Quantum Monte-Carlo calculation $\xi_n = 0.52$ in [28]. This yields the Landau parameters $F_0^s = \xi_n m^*/m - 1 = -0.42$ and $F_1^s = 3(m^*/m - 1) = 0.39$.

In the lowest temperature points (Fig. 3c) we observe a sudden deviation of the data from the fit (4) at $(k_BT/\mu)_c = 0.32(3)$ (see supplementary materials). We interpret this behavior as the transition from the normal phase to the superfluid phase. This critical ratio has been extensively calculated in the recent years. Our value is in close agreement with the diagrammatic Monte-Carlo calculation $(k_BT/\mu)_c = 0.32(2)$ of [6] and with the Quantum Monte-Carlo calculation $(k_BT/\mu)_c = 0.35(3)$ of [28] but differs from the self-consistent approach in [8] giving $(k_BT/\mu)_c = 0.41$, from the renormalization group prediction 0.24 in [29], and from several other less precise theories. From eq. (4) we deduce the total density $n = n_1 + n_2 = \partial P(\mu_i = \mu, T)/\partial\mu$ and the Fermi energy $E_F = k_BT_F = \hbar^2/2m(3\pi^2 n)^{2/3}$ at the transition point. We obtain $(\mu/E_F)_c = 0.49(2)$ and $(T/T_F)_c$=0.157(15), in very good agreement with [6]. Our measurement is

the first direct determination of $(\mu/E_F)_c$ and $(T/T_F)_c$ in the homogeneous gas. It agrees with the extrapolated value of the MIT measurement [19].

Below T_c, advanced theories [7, 8] predict that $P(\mu,T)/2P_1(\mu,0)$ is nearly constant (Fig. 3b). Therefore at $T=T_c$, $P/2P_1 \simeq \xi_s^{-3/2} \simeq 3.7$, and is consistent with our data. Here $\xi_s = 0.42(1)$ is the fundamental parameter characterizing the EOS of the balanced superfluid at zero temperature, a quantity extensively measured and computed in the recent years [2].

Our data is compared at all temperatures with the calculations from [6–9] (Fig.3a). The agreement with [7] is very good for a large range of temperatures. Concerning [6], the deviation with our data is about one error bar of the Monte-Carlo method below $\zeta = 0.2$ and the deviation increases with temperature (Fig. 3a). Furthermore, we show in the supplementary material that $h(1,\zeta)/2$ must be greater than 1, an inequality violated by the two hottest Monte-Carlo points of [6].

From our homogeneous EOS we can deduce the equation of state of the harmonically trapped unitary gas by integrating $h(1,\zeta)$ over the trap (see supplementary material). In particular, we find a critical temperature for the trapped gas $(T/T_F)_c = 0.19(2)$, where $T_F = \hbar(3\omega_r^2\omega_z N)^{1/3}$. This value agrees very well with the recent measurement of [30], and with less precise measurements [5, 31, 32].

Let us now explore a second line in the universal diagram $h(\eta,\zeta)$ (Fig. 1) by considering the case of the $T=0$ spin-imbalanced mixture $\mu_2 \neq \mu_1$, *i.e.* $\eta \neq 1$. Previous work [16–18] has shown that phase separation occurs in a trap. Below a critical population imbalance a fully-paired superfluid occupies the center of the trap. It is surrounded by a normal mixed phase and an outer rim consisting of an ideal gas of the majority component. In two out of the three previous experiments including ours [16, 18], the local density approximation has been carefully checked. We are therefore entitled to use (3) to analyze our data.

As in the previous case, the relationship between the pressure and the EOS requires the knowledge of the chemical potentials μ_1^0 and μ_2^0 at the center of the trap.

μ_1^0 is determined using the outer shell of the majority spin component ($i=1$). The pressure profile $P(\mu_{1z},\mu_{2z},0)$ corresponds to the Fermi-Dirac distribution and is fitted with the Thomas-Fermi formula $P_1 = \alpha(1-z^2/R_1^2)^{5/2}$, providing $\mu_1^0 = \frac{1}{2}m\omega_z^2 R_1^2$. Using P_1 for the calculation of $h = P/P_1$ cancels many systematic effects on the absolute value of the pressure. Moreover, fitting the outer shell using a finite-temperature Thomas-Fermi profile [19], we measure a temperature $k_BT = 0.03(3)\mu_1^0$.

μ_2^0 is fitted by comparison in the superfluid region with the superfluid equation of state at zero temperature [21]:

$$h(\eta,0) = (1+\eta)^{5/2}/(2\xi_s)^{3/2}. \qquad (5)$$

Our measured equation of state $h(\eta,0)$ is displayed in Fig.4. By construction our data agrees for $\eta \gtrsim 0.1$ with eq.(5). In Fig.4 the slope of $h(\eta,0)$ displays an obvious discontinuity for $\eta = \eta_c = 0.065(20)$. This is a signature of a first-order quantum phase transition to the partially polarized normal phase. The error bar is dominated by the uncertainty on ξ_s. This value is slightly higher than the prediction $\eta_c = 0.02$ given by the fixed-node Monte-Carlo [10] and than the value $\eta_c = 0.03(2)$ measured in [19].

From the relations $n_i = \partial P/\partial\mu_i$ we deduce from $h(\eta,0)$

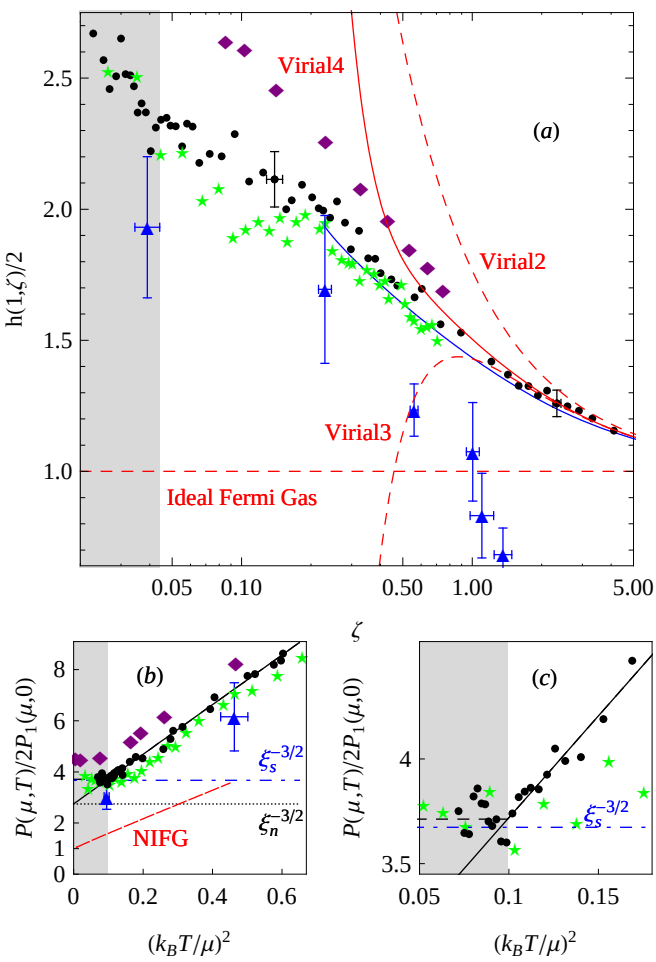

FIG. 3: (color online) Equation of state of a spin-balanced unitary Fermi gas. (a) Finite-temperature equation of state $h(1,\zeta)$ (black dots). The error bars represented at $\zeta = 0.14$ and $\zeta = 2.3$ indicate the 6% accuracy in ζ and h of our EOS. The red curves are the successive virial expansions up to 4^{th} order. The blue triangles are from [6], the green stars from [7], the purple diamonds from [8], and the blue solid line from [9]. The grey region indicates the superfluid phase. (b) Equation of state $P(\mu,T)/2P_1(\mu,0)$ as a function of $(k_BT/\mu)^2$, fitted by the Fermi liquid equation of state (4). The red dashed line is the non-interacting Fermi gas (NIFG). The horizontal dot-dashed (resp. dotted) line indicates the zero-temperature pressure of the superfluid phase $\propto \xi_s^{-3/2}$ (resp. normal phase $\propto \xi_n^{-3/2}$). (c) Expanded view of (b) near T_c. The sudden deviation of the data from the fit occurs at $(k_BT/\mu)_c = 0.32(3)$ that we interpret as the superfluid transition. The black dashed line indicates the mean value of the data points below T_c.

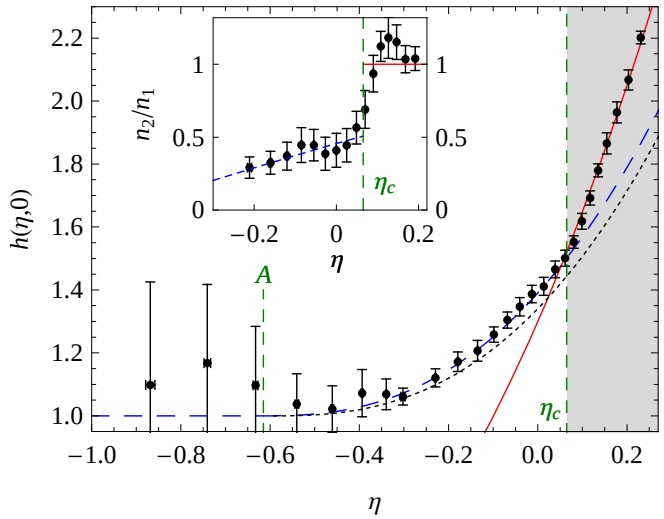

FIG. 4: (color online) Equation of state of the zero-temperature spin-imbalanced unitary gas $h(\eta, 0)$ (black dots). Error bars are equal to one standard error. The red solid line is the superfluid equation of state, the blue dashed line is the ideal Fermi liquid equation (7) with $A = -0.615$, $m^* = 1.20m$ and the black dotted line is the Monte Carlo calculation from [10]. Inset: Local density ratio n_2/n_1 as a function of η. The red solid line $n_2/n_1 = 1$ corresponds to the fully paired superfluid and blue dashed line to the model (7).

the density ratio n_2/n_1 (see inset in Fig.4). This ratio is discontinuous at the phase transition, from a maximum value in the normal phase $(n_2/n_1)_c = 0.5(1)$ to $n_2 = n_1$ in the superfluid phase. Our value is close to the zero-temperature calculation 0.44 [10] and agrees with the coldest MIT samples [19, 20]. It confirms that the temperature is much smaller than the tricritical point temperature $T = 0.07T_F$ [19] where the discontinuity vanishes, justifying our $T = 0$ assumption made above.

For $\eta < \eta_c$ our data displays a good agreement with a simple polaron model, based on the pioneering work in [10]. A polaron is a quasi-particle describing a single minority atom immersed in the majority Fermi sea [15, 18, 21, 22]. It is characterized by a renormalized chemical potential $\mu_2 - A\,\mu_1$ and an effective mass m_p^* [10]. Following this picture, we write the pressure as the sum of the Fermi pressures of ideal gases of majority atoms and of polarons:

$$P = \frac{1}{15\pi^2}\left(\frac{2m}{\hbar^2}\right)^{3/2}\left(\mu_1^{5/2} + \left(\frac{m_p^*}{m}\right)^{3/2}(\mu_2 - A\mu_1)^{5/2}\right), \quad (6)$$

which can be written as

$$h(\eta, 0) = 1 + \left(\frac{m_p^*}{m}\right)^{3/2}(\eta - A)^{5/2}. \quad (7)$$

A and m_p^* have recently been calculated exactly [14, 15]: $A = -0.615$, $m_p^*/m = 1.20(2)$ and with these values inserted in (7) the agreement with our data is perfect. Note that our data lies slightly above the variational fixed-node Monte Carlo calculation [10]. We therefore conclude that interactions between polarons are not visible at this level of precision.

b_3	b_4	$(k_BT/\mu)_c$	$(\mu/E_F)_c$	$(T/T_F)_c$
-0.35(2)	0.096(15)	0.32(3)	0.49(2)	0.157(15)
ξ_n	m^*/m	η_c	$(n_2/n_1)_c$	m_p^*/m
0.51(2)	1.13(3)	0.065(20)	0.5(1)	1.20(2)

TABLE I: Table of quantities measured in this work.

Alternatively, we can fit our data with m_p^*/m as a free parameter in (7). We obtain $m_p^*/m = 1.20(2)$. The uncertainty combines the standard error of the fit and the uncertainty on ξ_s. This value agrees with our previous measurement $m_p^*/m = 1.17(10)$ [18] (with a 5-fold improvement in precision), with the theoretical value $m_p^*/m = 1.20(2)$ in [14, 15] and with the variational calculation [13]. It differs from the values 1.09(2) in [33], 1.04(3) in [10], and from the experimental value 1.06 in [20].

We arrive at a simple physical picture of the $T = 0$ spin-polarized gas: the fully paired superfluid is described by an ideal gas EOS renormalized by a single coefficient ξ_s; the normal phase is nothing but two ideal gases, one of bare majority particles and one of polaronic quasi-particles.

In conclusion, we have introduced a powerful method for the measurement of the equation of state of the unitary and homogeneous Fermi gas, that enables direct comparison with theoretical models and provides a set of new parameters shown in Tab.I. The method can readily be extended to any multi-component cold atom gas in three dimensions that fulfills the local density approximation (see supplementary discussion). We have shown that the normal phase of the unitary Fermi gas is a strongly correlated system whose thermodynamic properties are well described by Fermi liquid theory, unlike high-T_c cuprates.

Note added in proof: Since this paper was accepted for publication, we have become aware of the measurement of a similar equation of state for the balanced unitary Fermi gas at finite temperature by different methods [34].

METHODS SUMMARY

Our experimental setup is presented in [18]. We load into an optical dipole trap and evaporate a mixture of ^{6}Li in the $|1/2, \pm 1/2\rangle$ states and of ^{7}Li in the $|1, 1\rangle$ state at 834 G. The cloud typically contains $N_6 = 5$ to 10×10^4 ^{6}Li atoms in each spin state and $N_7 = 3$ to 20×10^3 ^{7}Li atoms at a temperature from $T = 150$ nK to 1.3 μK. The ^{6}Li trap frequencies are $\omega_z/2\pi = 37$ Hz, $\omega_r/2\pi$ varying from 830 Hz to 2.20 kHz, and the trap depth is 25 μK for our hottest samples, with $T \simeq 2T_F$. ^{6}Li atoms are imaged *in situ* using absorption imaging, while ^{7}Li atoms are imaged after time of flight, providing the temperature in the same experimental run (Fig. 4). Since the scattering length describing the interaction between ^{7}Li and ^{6}Li atoms, $a_{67} = 2$ nm, is much smaller than k_F^{-1}, the ^{7}Li thermometer has no influence on the ^{6}Li density

profiles. The ^{7}Li-^{6}Li collision rate, $\Gamma_{67} = 10\ \mathrm{s}^{-1}$, is large enough to ensure thermal equilibrium between the two species.

[1] Ho, T.-L. Universal thermodynamics of degenerate quantum gases in the unitarity limit. *Phys. Rev. Lett.* **92**, 90402 (2004).

[2] Inguscio, M., Ketterle, W. & Salomon, C. Ultracold Fermi Gases. *Proceedings of the International School of Physics Enrico Fermi, Course CLXIV, Varenna* (2006).

[3] Stewart, J., Gaebler, J., Regal, C. & Jin, D. Potential Energy of a ^{40}K Fermi Gas in the BCS-BEC Crossover. *Phys. Rev. Lett.* **97**, 220406 (2006).

[4] Luo, L., Clancy, B., Joseph, J., Kinast, J. & Thomas, J. Measurement of the entropy and critical temperature of a strongly interacting Fermi gas. *Phys. Rev. Lett.* **98**, 80402 (2007).

[5] Luo, L. & Thomas, J. Thermodynamic Measurements in a Strongly Interacting Fermi Gas. *J. Low Temp. Phys.* **154**, 1–29 (2009).

[6] Burovski, E., Prokofev, N., Svistunov, B. & Troyer, M. Critical temperature and thermodynamics of attractive fermions at unitarity. *Phys. Rev. Lett.* **96**, 160402 (2006).

[7] Bulgac, A., Drut, J. & Magierski, P. Spin 1/2 fermions in the unitary regime: A superfluid of a new type. *Phys. Rev. Lett.* **96**, 90404 (2006).

[8] Haussmann, R., Rantner, W., Cerrito, S. & Zwerger, W. Thermodynamics of the BCS-BEC crossover. *Phys. Rev. A* **75**, 23610 (2007).

[9] Combescot, R., Alzetto, F. & Leyronas, X. Particle distribution tail and related energy formula. *Phys. Rev. A* **79**, 053640 (2009).

[10] Lobo, C., Recati, A., Giorgini, S. & Stringari, S. Normal state of a polarized Fermi gas at unitarity. *Phys. Rev. Lett.* **97**, 200403 (2006).

[11] Liu, X., Hu, H. & Drummond, P. Virial expansion for a strongly correlated Fermi gas. *Phys. Rev. Lett.* **102**, 160401 (2009).

[12] Rupak, G. Universality in a 2-Component Fermi System at Finite Temperature. *Phys. Rev. Lett.* **98**, 90403 (2007).

[13] Combescot, R., Recati, A., Lobo, C. & Chevy, F. Normal state of highly polarized Fermi gases: simple many-body approaches. *Phys. Rev. Lett.* **98**, 180402 (2007).

[14] Combescot, R. & Giraud, S. Normal state of highly polarized Fermi gases: full many-body treatment. *Phys. Rev. Lett.* **101**, 050404 (2008).

[15] Prokof'ev, N. & Svistunov, B. Fermi-polaron problem: Diagrammatic monte carlo method for divergent sign-alternating series. *Phys. Rev. B* **77**, 020408 (2008).

[16] Shin, Y., Zwierlein, M., Schunck, C., Schirotzek, A. & Ketterle, W. Observation of phase separation in a strongly interacting imbalanced Fermi gas. *Phys. Rev. Lett.* **97**, 30401 (2006).

[17] Partridge, G., Li, W., Kamar, R., Liao, Y. & Hulet, R. Pairing and phase separation in a polarized Fermi gas. *Science* **311**, 503–505 (2006).

[18] Nascimbene, S. *et al.* Collective Oscillations of an Imbalanced Fermi Gas: Axial Compression Modes and Polaron Effective Mass. *Phys. Rev. Lett.* **103**, 170402 (2009).

[19] Shin, Y., Schunck, C., Schirotzek, A. & Ketterle, W. Phase diagram of a two-component Fermi gas with resonant interactions. *Nature* **451**, 689–693 (2008).

[20] Shin, Y. Determination of the equation of state of a polarized fermi gas at unitarity. *Phys. Rev. A* **77**, 041603 (2008).

[21] Chevy, F. Universal phase diagram of a strongly interacting fermi gas with unbalanced spin populations. *Phys. Rev. A* **74**, 063628 (2006).

[22] Schirotzek, A., Wu, C.-H., Sommer, A. & Zwierlein, M. W. Observation of fermi polarons in a tunable fermi liquid of ultracold atoms. *Phys. Rev. Lett.* **102**, 230402 (2009).

[23] Ho, T.-L. & Zhou, Q. Obtaining phase diagram and thermodynamic quantities of bulk systems from the densities of trapped gases. *Nature Phys.* **6**, 131 (2010).

[24] Spiegelhalder, F. *et al.* Collisional Stability of ^{40}K Immersed in a Strongly Interacting Fermi Gas of ^{6}Li. *Phys. Rev. Lett.* **103**, 223203 (2009).

[25] Ho, T.-L. & Mueller, E. High temperature expansion applied to fermions near Feshbach resonance. *Phys. Rev. Lett.* **92**, 160404 (2004).

[26] Chen, Q., Stajic, J., Tan, S. & Levin, K. BCS BEC crossover: From high temperature superconductors to ultracold superfluids. *Physics Reports* **412**, 1–88 (2005).

[27] Carlson, J., Chang, S., Pandharipande, V. & Schmidt, K. Superfluid Fermi gases with large scattering length. *Phys. Rev. Lett.* **91**, 50401 (2003).

[28] Bulgac, A., Drut, J. & Magierski, P. Quantum Monte Carlo simulations of the BCS-BEC crossover at finite temperature. *Phys. Rev. A* **78**, 23625 (2008).

[29] Gubbels, K. & Stoof, H. Renormalization group theory for the imbalanced Fermi gas. *Phys. Rev. Lett.* **100**, 140407 (2008).

[30] Riedl, S., Guajardo, E., Kohstall, C., Denschlag, J. & Grimm, R. Superfluid Quenching of the Moment of Inertia in a Strongly Interacting Fermi Gas. *arXiv:0907.3814* (2009).

[31] Greiner, M., Regal, C. & Jin, D. Emergence of a molecular Bose-Einstein condensate from a Fermi gas. *Nature* **426**, 537–540 (2003).

[32] Inada, Y. *et al.* Critical temperature and condensate fraction of a fermion pair condensate. *Phys. Rev. Lett.* **101**, 180406 (2008).

[33] Pilati, S. & Giorgini, S. Phase separation in a polarized Fermi gas at zero temperature. *Phys. Rev. Lett.* **100**, 030401 (2008).

[34] Horikoshi, M., Nakajima, S., Ueda, M.& Mukaiyama, T. Measurement of Universal Thermodynamic Functions for a Unitary Fermi Gas. *Science* **327**, 442 (2010).

[35] Feynman, R.P. Statistical Mechanics: A set of lectures. *Frontiers in Physics. New York* (1972).

Acknowledgements We are grateful to R. Combescot, X. Leyronas, Y. Castin, A. Recati, S. Stringari, S. Giorgini, M. Zwierlein and T. Giamarchi for fruitful discussions and to C. Cohen-Tannoudji, J. Dalibard, F. Gerbier and G. Shlyapnikov for critical reading of the manuscript. We acknowledge support from ESF (Euroquam), SCALA, ANR FABIOLA, Région Ile de France (IFRAF), ERC and Institut Universitaire de France.

Author Contributions S. Nascimbène and N. Navon contributed equally to this work. S.N., N.N. and K.J. took the experimental data and all authors contributed to the data analysis and writing of the manuscript.

Author Information Correspondence and requests for materials should be addressed to S. N. (email:sylvain.nascimbene@ens.fr).

METHODS

Construction of the equation of state by successive patches. A typical image at high temperature provides about 100 pixels corresponding to ζ values varying from 2 at the trap center to 6 at the edges, with a signal-to-noise from 3 to 10. 7 such images are fitted in the wings using the second-order virial expansion and averaged to obtain a low-noise EOS up to $\zeta = 2$. Then images of clouds where the evaporation has been pushed to a slightly lower temperature are recorded. They show about 75% overlap in ζ with the previous EOS. After minimization of the distance between a new image and the previously determined EOS in the overlap region, we obtain the value of μ^0 for a single image with 3% statistical uncertainty. This process is repeated for 6 successive trap depths. When averaging one image with typically 10 previous images, we obtain a new EOS with an error on ζ of about $0.03/\sqrt{10} \simeq 1\%$. The EOS experiences a random walk error on the 40 images of $0.01 \times \sqrt{40} \simeq 5\%$ for the coldest data. An independent check of the maximum error is provided by the good agreement with the superfluid equation of state for temperatures lower than T_c [7, 8].

Evaluation of the systematic uncertainties. For the measurement of $h(1, \zeta)$, the combined uncertainties on the radial frequency of the trap, trap anharmonicity, magnification of our imaging system, and atom counting affect the pressure measurement given in (3) at $\simeq 20\%$ level. However, two measurements, one at relatively high temperature and one at very low temperature, enable us to show that the overall error does not exceed 6%. In the temperature range $\zeta > 0.5$, the agreement between the experimental value $b_3 = -0.35(2)$ and the theoretical value $b_3 = -0.355$ of the third virial coefficient indicates that the global systematic error is smaller than 6%. Second, at very low temperature, theory [7, 8] predicts that the variation of $P/2P_1$ as a function of k_BT/μ in the superfluid phase remains smaller than 5%. Our value of $P/2P_1 = 3.75$ below the critical point is within 5% of the $T = 0$ prediction $\xi_s^{-3/2} = 3.7(2)$. This confirms that systematic errors for our coldest samples are also smaller than 6%.

For the determination of the critical transition to superfluidity we fit the low-temperature data $P(\mu, T)/2P_1(\mu, 0)$ with a variable horizontal line for $T < T_c$ and with the Fermi-liquid equation (4) for $T > T_c$. The result of the fit is the dashed black line in Fig. 3c, which intersects equation (4) at $(k_BT/\mu)_c = 0.315(8)$. This statistical error is negligible compared to the error induced by the 6% systematic uncertainty discussed above, justifying our very simplified fit procedure. Indeed a 6% error on the pressure induces a 10% error on μ for images recorded in the vicinity of the critical temperature, leading to $(k_BT/\mu)_c = 0.32(3)$.

For the measurement of $h(\eta, 0)$, the fit of the fully polarized wings of the cloud serves as a pressure calibration for the rest of the cloud, cancelling many systematic effects.

In order to estimate temperature effects in the polarized gas, let us first remark that in the superfluid phase corrections scale as T^4 for the bosonic excitations and are exponentially suppressed by the gap for the fermionic ones [7]. So in our temperature range $k_BT = 0.03\mu_1^0$ their contributions will be very small. On the other hand, in the partially polarized normal phase, we expect a typical Fermi liquid T^2 scaling. In order to obtain an estimate of the error on the EOS, we develop the following simple model. In equation (9) which describes a mixture of zero-temperature ideal gases, we replace the Fermi pressures by the finite-temperature pressures of ideal gases (see equation (1)):

$$P(\mu_1, \mu_2, T) = P_1(\mu_1, T) + \left(\frac{m_p^*}{m}\right)^{3/2} P_1(\mu_2 - A\mu_1, T),$$

and run the analysis described in the main text. At $T = 0.05\mu_1^0$, the correction on h is less than 1%, half of our current error bar.

Limit of ^{7}Li Thermometry. As the scattering length between the ^{7}Li atoms, $a_{77} = -3$ nm is negative, the ^{7}Li cloud becomes unstable when a BEC forms. This occurs at $T \sim 150$ nK with typically 3500 atoms. Precise thermometry with lower atom numbers becomes difficult. For the measurement of the zero-temperature equation of state of the imbalanced gas, we do not use ^{7}Li thermometry but rather the fit of the wings of the majority spin component.

SUPPLEMENTARY DISCUSSION

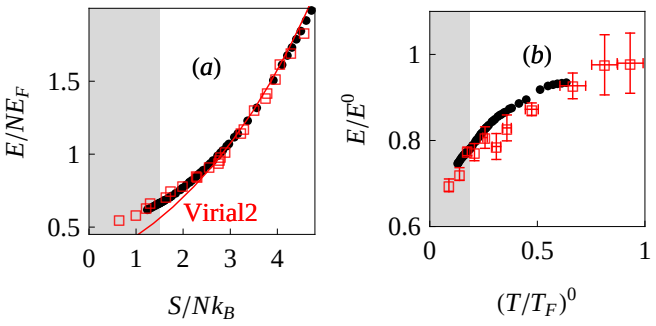

FIG. 5: (color online) Equations of state of the trapped unitary gas. (a) Comparison between our EOS E/NE_F as a function of S/Nk_B (black dots) and the EOS measured in [5] (open red squares). The red solid line is the second-order virial equation of state. (b) Comparison between our EOS E/E^0 as a function of $(T/T_F)^0$ (black dots) and the EOS measured on ^{40}K in [3] (open red squares). The grey regions correspond to the superfluid phase.

Equation of State of the Trapped Unitary Gas

In this work, we have measured the equation of state of the homogeneous unitary gas. We can deduce from our data the EOS of the trapped balanced unitary gas, which has been measured in [3, 5].

Using the local density approximation, the total atom number $N = \int n\,\mathrm{d}r^3$ is expressed as a function of the temperature T and the chemical potential μ^0 at the center, involving the function $h(1,\zeta)$:

$$N = \frac{-2}{\sqrt{\pi}}\left(\frac{k_BT}{\hbar\omega}\right)^3 \int_{\zeta_0}^{\infty} \frac{\mathrm{d}\log^{1/2}(\zeta/\zeta_0)}{\mathrm{d}\zeta} f_{5/2}(-\zeta^{-1})h(\zeta)\mathrm{d}\zeta, \tag{8}$$

where $\zeta_0 = \exp(-\mu^0/k_BT)$ and $\omega = (\omega_r^2\omega_z)^{1/3}$. We use for the calculation a discretized version of (8) taken solely on our experimental values of h, *i.e.* without using any interpolating or fitting function. Similar expressions are used to calculate the Fermi temperature $E_F = k_BT_F = \hbar\omega(3N)^{1/3}$, the total entropy S and energy E of the cloud. The equation of state E/NE_F as a function of S/Nk_B, displayed in Supplementary Fig.5a, is in very good agreement with [5].

The normal-superfluid phase transition for the trapped gas occurs when at the trap center $\zeta_0 = \zeta_c = \exp(-(k_BT/\mu)_c^{-1})$, with $(k_BT/\mu)_c = 0.32(3)$, as measured on the homogeneous EOS $h(1,\zeta)$. At this point we get $(T/T_F)_c = 0.19(2)$, $(S/Nk_B)_c = 1.5(1)$ and $(E/NE_F)_c = 0.67(5)$.

In order to make the comparison with [3], we also express the equation of state E/E^0 as a function of $(T/T_F)^0$, where the superscript ^{0} refers to the quantities evaluated on a non-interacting Fermi gas having the same entropy (Supplementary Fig.5b). The good agreement with the measurement in [3], performed on ^{40}K clouds, illustrates the universality of the unitary gas.

Physical interpretation of the pressure in the normal mixed phase

We have shown that the pressure in the normal mixed phase can be described as the sum of the Fermi pressures of ideal gases of majority atoms and of polarons:

$$P = \frac{1}{15\pi^2}\left(\frac{2m}{\hbar^2}\right)^{3/2}\left(\mu_1^{5/2} + \left(\frac{m_p^*}{m}\right)^{3/2}(\mu_2 - A\mu_1)^{5/2}\right). \tag{9}$$

Here, we evaluate the corresponding canonical EOS relating the energy E to the densities n_1, n_2, in order to compare with the Fixed Node Monte Carlo prediction [10]. Since at unitarity we have $E = 3PV/2$ [1], we just express the chemical potentials in terms of densities by using the thermodynamical identities $n_i = \partial_{\mu_i}P$, which yield respectively:

$$n_2 = \frac{1}{6\pi^2}\left[\frac{2m^*}{\hbar^2}(\mu_2 - A\mu_1)\right]^{3/2} \tag{10}$$

$$n_1 = \frac{1}{6\pi^2}\left(\frac{2m\mu_1}{\hbar^2}\right)^{3/2} - An_2. \tag{11}$$

The last term in equation (11) clearly indicates the increased majority density due to the presence of the minority component. Expressing the pressure as a function of n_i in (9) yields the energy:

$$E = E_{\mathrm{FP}}\left[(1+Ax)^{5/3} + \frac{m}{m^*}x^{5/3}\right],$$

where E_{FP} is the energy of the fully polarized gas and $x = n_2/n_1$. Expanding E to order x^2 finally leads to an expression similar to that obtained in [10]:

$$E(x) = E_{\mathrm{FP}}\left(1 + \frac{5}{3}Ax + \frac{m}{m^*}x^{5/3} + Bx^2 + ...\right),$$

with $B = 5A^2/9 = 0.2$. Our value of B is close to the calculated value $B \simeq 0.14$ from [10].

Trap Anharmonicity

First, in the axial direction z, the confinement is produced magnetically and the corresponding anharmonicity is negligible. In the radial direction, we develop the gaussian potential to fourth order around $\rho = 0$:

$$V_r(\rho) = V_0\left(1 - \exp\frac{-\rho^2}{\sigma^2}\right) \simeq \frac{1}{2}m\omega_r^2\rho^2 + \epsilon\rho^4,$$

where $m\omega_r^2 = 2V_0/\sigma^2$ and $\epsilon = -V_0/2\sigma^4$. In the balanced case, we have

$$\overline{n}(z) = \int \mathrm{d}^2\rho\, n\left(\mu^0 - \frac{1}{2}m\omega_z^2 z^2 - \frac{1}{2}m\omega_r^2\rho^2 - \epsilon\rho^4\right).$$

Introducing $n = \partial P/\partial\mu$ and defining $u = m\omega_r^2\rho^2/2 + \epsilon\rho^4$ we obtain, to lowest order,

$$\frac{m\omega_r^2}{2\pi}\overline{n}(z) = P(\mu_z) + \int_0^\infty P(\mu_z - u)\frac{\mathrm{d}u}{V_0}.$$

The error on the measurement of h is then

$$\frac{m\omega_r^2\,\overline{n}(z)}{2\pi P_1(\mu_z, T)} - h(1,\zeta) = \frac{k_B T}{V_0}\int_\zeta^\infty \frac{f_{5/2}(-\zeta'^{-1})}{f_{5/2}(-\zeta^{-1})}\frac{h(1,\zeta')}{\zeta'}\mathrm{d}\zeta'. \tag{12}$$

We evaluate the integral in (12) using the experimental values of $h(1,\zeta)$. In our shallowest trap, the worst case anharmonicity effect is 5%.

An exact inequality on the equation of state of an attractive Fermi gas

Writing the hamiltonian as $\widehat{H} = \widehat{H}_0 + \widehat{U}$, where $\widehat{H}_0$ is the single-particle part of the hamiltonian and $\widehat{U}$ is the inter-particle interaction, one has the general inequality $\Omega \leq \Omega_0 + \langle V\rangle_0$, where Ω_0 is the grand potential associated with $\widehat{H}_0$ and $\langle\cdot\rangle_0$ is the thermal average related to $\widehat{H}_0$ [35]. Taking for U a short range square potential of depth $U_0 < 0$ recovering the true scattering length, one has trivially $\langle\widehat{V}\rangle_0 < 0$, hence $\Omega \leq \Omega_0$. Using the thermodynamic identity $\Omega = -PV$, and recalling that $\Omega_0 = -2P_1 V$ and $h = P/P_1$, we finally get the inequality

$$h(1,\zeta) \geq 2.$$

Extension to a Multi-Component System

We extend the equation (2) to a mixture of species i, of mass m_i, trapped in a harmonic trap of transverse frequencies ω_{ri}, following the calculations in [23]. Using Gibbs-Duhem relation at a constant temperature T, $\mathrm{d}P = \sum_i n_i \mathrm{d}\mu_i$, then

$$\sum_i \frac{m_i\omega_{ri}^2}{2\pi}\overline{n}_i = \int\sum_i \frac{m_i\omega_{ri}^2}{2\pi}\mathrm{d}x\mathrm{d}y\frac{\partial P}{\partial\mu_i} = \int\sum_i \mathrm{d}\mu_i\frac{\partial P}{\partial\mu_i},$$

where we have used local density approximation ($\mu_i(\mathbf{r}) = \mu_i^0 - V(\mathbf{r})$) to convert the integral over space to an integral on the chemical potentials. The integral is straightforward and yields to

$$P(\mu_{iz}, T) = \frac{1}{2\pi}\sum_i m_i\omega_{ri}^2\overline{n}_i(z).$$